(Received 8 April 2025, Accepted 30 April 2025, Scheduled 6 June 2025)

Intra- and Peritumoral Radiomics-Based Models for Preoperative Prediction of Lymphatic Vascular Invasion in Invasive Breast Cancer

Lingxia Wang[1], Weixing Pan[2], Yitian Wu[3], Huangqi Zhang[2], Aie Liu[4], Enhui Xin[4], Jiadong Zhang[5], Lei Chen[4], Hongjie Hu[7,*], and Wenbin Ji[1,6,*]

[1]*Department of Radiology, Taizhou Hospital of Zhejiang Province, Zhejiang University, Taizhou 317000, Zhejiang, China*
[2]*Department of Radiology, Taizhou Hospital of Zhejiang Province affiliated to Wenzhou Medical University Linhai 317000, Zhejiang, China*
[3]*School of Medicine, Shaoxing University, Shaoxing 312000, Zhejiang, China*
[4]*Department of Research Center, Shanghai United Imaging Intelligence Co., Ltd., China*
[5]*School of Biomedical Engineering, ShanghaiTech University, Shanghai 201210, China*
[6]*Key Laboratory of Evidence-based Radiology of Taizhou, Linhai 317000, Zhejiang, China*
[7]*Department of Radiology, Sir Run Run Shaw Hospital, Zhejiang University School of Medicine, Hangzhou 310016, China*

ABSTRACT: In this study, we evaluated the feasibility of intra- and peritumoral artificial intelligence (AI)-based radiomics from dynamic contrast-enhanced magnetic resonance imaging (DCE-MRI) for preoperative prediction of lymphatic vascular invasion (LVI) in invasive breast cancer (IBC). Our results demonstrated that a radiomic model (area under the receiver operating characteristic curve AUC $= 0.951$) outperformed a clinical model (AUC $= 0.644$) in 193 patients. Optimal tumor segmentation using 3D RU-Net (Dice score > 0.75) and 3 mm to 4 mm isotropic 3D peritumoral expansion yielded the strongest predictive performance.

1. INTRODUCTION

According to the 2022 global cancer statistics, breast cancer was the second most common cancer, accounting for 11.6% of total cancer cases [1]. Recent studies have shown that lymphatic vascular invasion (LVI) by tumors is an essential prognostic factor affecting patient outcomes and clinical treatment decisions [2–4]. LVI is the invasion of tumor emboli into the lymphatic space, blood vessels, or both around the tumor [4]. LVI, which can manifest as lymph node metastasis, is associated with an elevated risk of lymphatic metastasis resulting from tumor-related lymphangiogenesis [5]. One of the leading causes of breast cancer-related death is lymph node metastasis [6]. Therefore, LVI is considered one of the main reference criteria for tumor staging, prognostic prediction, and treatment decisions [7, 8]. However, during clinical diagnosis, postoperative pathology is currently the only available tool to confirm that tumors promote lymphatic and blood vessel growth and invasion, and there is no effective way to predict LVI status before surgery noninvasively.

Radiomics provides a new method and tool for clinical tumor diagnosis, treatment decisions, and prognosis prediction [9]. Four previous studies applied MRI-based intratumoral radiomics to predict LVI status in patients with breast cancer [10–13]; However, their results were controversial. Liu et al. determined that a model combining the radiometric features based on Dynamic contrast-enhanced magnetic resonance imaging (DCE-MRI) and the status of axillary lymph nodes (ALN) could better predict LVI status, with an area under the curve (AUC) of 0.763 [10]. Kayadibi et al. established a radiomic model based on the apparent diffusion coefficient (ADC) with an AUC of 0.732 [13]. Zhang et al. found that fusion radiomic models of T2-weighted imaging (T2WI), contra-enhanced T1-weighted imaging (DCE), and ADC images predicted LVI status better than any of them alone [11]. Nijiati et al.'s ADC radiomics model achieved an area under the receiver operating characteristic curve (AUC) of 0.77 [12]. The studies mentioned above delineated the intratumoral regions for analysis of imaging characteristics while neglecting the examination of imaging features in the peritumoral areas. Most contemporary studies [14–16] have established intratumoral and peritumoral radiomic models for preoperative prediction of HER-2 Status, molecular subtypes of ALN metastasis, etc. At present, only Jiang et al. [17] have developed a nomogram to evaluate the intra- and peritumoral radiomics for assessing LVI.

In radiomics analysis, accurate region-of-interest (ROI) delineation is critical for extracting quantitative imaging features. However, manual segmentation of breast lesions in DCE-MRI is time-consuming and prone to interobserver variability, prompting the development of automated and semi-automated segmentation algorithms. Recent advancements include several notable approaches: Lee et al. [18] introduced an active contour-based skin segmentation method to remove superficial tissues in DCE-MRI, achieving a Dice coefficient of 93.2%

* Corresponding authors: Wenbin Ji (wb.j@163.com); Hongjie Hu (hongjiehu@zju.edu.cn).

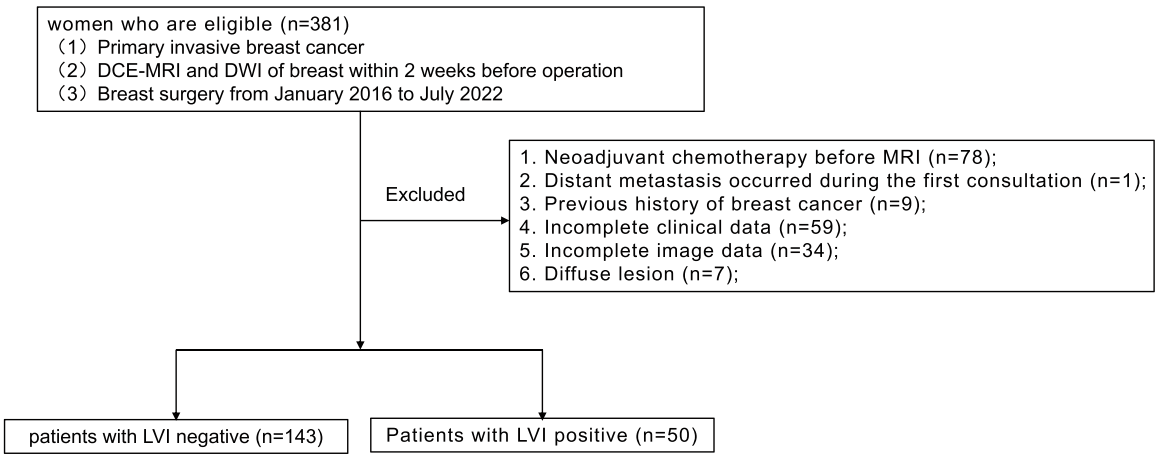

FIGURE 1. Flowchart of study population. DCE-MRI, dynamic contrast enhancement-magnetic resonance imaging; DWI, diffusion weighted imaging.

for 3D reconstructed images and demonstrating superior speed and accuracy compared to manual segmentation. Khaled et al. [19] developed a U-Net ensemble framework that combines three models with different input configurations, achieving a mean Dice similarity coefficient (DSC) of 0.680 on the TCGA-BRCA dataset and highlighting the value of multi-input feature fusion in complex imaging scenarios. Si et al. [20] proposed a Chimp Optimization Algorithm (CHOA) for multilevel thresholding, achieving DSCs of 87.09% without opposition-based learning and 93.25% with this technique, outperforming traditional optimization methods in sensitivity, accuracy, and noise robustness. To address the challenges of segmenting breast tumors with variable shapes/sizes and inhomogeneous backgrounds in DCE-MR images, this study [21] proposes a tumor-sensitive synthesis module that integrates differential loss feedback to suppress false positives and enhance boundary accuracy, validated on a large 422-subject dataset to demonstrate improved segmentation effectiveness, adaptability, and robustness. Si and Mukhopadhyay [22] introduced a fireworks algorithm-based clustering approach with preprocessing for denoising and intensity correction, demonstrating higher DSC values and lower computational complexity than particle swarm optimization or k-means. A recent study has observed that the peritumoral regions closely related to tumors have radiomic characteristics related to prognosis, which may help further clarify tumor heterogeneity [23]. Patients with LVI-positive have a greater risk of local recurrence and distant metastasis [24]. Therefore, noninvasive methods to predict LVI-positive status in breast cancer have important clinical implications for early detection of the disease. In this study, we aimed to develop and validate semi-automated 3D intra- and peritumoral radiomics models using preoperative DCE-MRI as a noninvasive tool for predicting LVI status in patients with breast cancer.

2. MATERIALS AND METHODS

2.1. Patients Selection

This retrospective study included 193 patients (197 lesions) with invasive breast cancer (IBC) diagnosed by surgical resection between January 2016 and July 2022. Figure 1 depicts the flowchart illustrating the enrollment process of the study population. The inclusion criteria were as follows: (1) histopathological evaluation of surgical specimens in patients with recently diagnosed IBC; and (2) underwent breast mass surgery within two weeks after MRI scanning. An additional 188 patients were excluded owing to various reasons, such as neoadjuvant chemotherapy before MRI, distant metastasis occurring during the first consultation, previous breast cancer history, incomplete clinical or imaging data, and diffuse lesions. For patients with multiple lesions, only the largest lesions were included in this study. The CT results were evaluated based on the American Radiological Society Breast Imaging Report and Data System.

2.2. Histopathological Analyses

Histopathological and immunohistochemical data were obtained from the surgical pathology reports. Tissue analysis was performed on the samples obtained from surgery. LVI was evaluated on hematoxylin and eosin-stained sections and defined as cancer cells in a certain endothelial lining space around the IBC [9]. The reported criteria for estrogen receptor (ER) and progesterone receptor (PR) status are as follows: $<$ 1% reactive cells are negative, and $\geq$ 1% reactive cells are positive. The IHC staining standard score of HER-2 is 0, 1+, 2+, or 3+, among which 0 and 1+ are negative, and 3+ is positive. Fluorescence in situ hybridization for HER-2 amplification was performed when the HER-2 score was 2+. A positive result of fluorescence in situ hybridization amplification was regarded as HER-2 positive. Ki-67 is divided into two categories with 14% as the boundary: $\geq$ 14% and $<$ 14%. Histological grade was carried out using the method of Elston and Ellis [25]. IBC is usually classified into three grades: Grade I (highly differentiated), Grade II (moderately differentiated), and Grade III (poorly differentiated).

2.3. MRI Acquisition

The examinations were performed using a 1.5 T MR (Signa HDxt 1.5T, GE Healthcare, USA) or a 3.0 T MR scanner

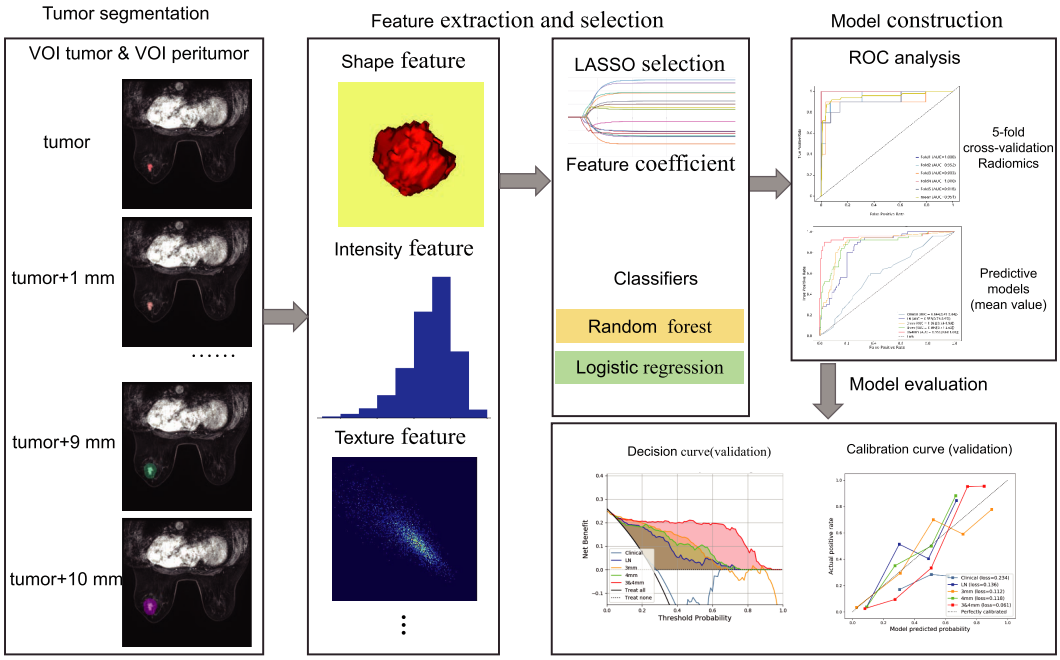

FIGURE 2. Flowcharts radiomics analysis. VOI, volumetric interest (volume of interest); LASSO, Least absolute shrinkage and selection operator; ROC, receiver operating characteristic curve; VOI tumor, the three-dimensional volume of the whole tumor; $VOI_{1\,mm}$, $VOI_{2\,mm}$, …, and $VOI_{10\,mm}$, performing an isometric 3D expansion of the intratumoral region (VOI_{tumor}) from 1 mm to 10 mm resulted in the generation of regions including both the tumor and the peritumor, which were labeled as $VOI_{1\,mm}$, $VOI_{2\,mm}$, …, and $VOI_{10\,mm}$, respectively.

(Discover MR 750 3.0T, GE Healthcare, USA) and a special phased-array surface coil for the breast. The patients were placed in a prone position with a unilateral breast naturally suspended in a breast coil for scanning. Axial lava sequence scanning was performed to obtain DCE-MRI. The contrast agent was gadopentetate dimeglumine (Guangzhou Kangshen Pharmaceutical Co., Ltd., China). The dose of intravenous bolus injection was 0.1 mmol/kg, and the rate was 2.5 mL/s. After the contrast agent was injected, 20 mL of normal saline was injected at the same rate. A mask was acquired before the enhancement. Fifteen seconds after the contrast agent was injected, scanning was performed seven consecutive times.

DCE-MRI comprised a total of eight stages, with a single scan time of 51 s in 3.0 T MRI. The first four stages were separated by 1 s, and the 5th, 6th, and 7th stages were separated by 60 s, with a total scan time of 9 min and 51 s. The scanning parameters were as follows: repetition time (TR) 3.9 ms, echo time (TE) 2.2 ms, flip angle (FA) 5°, FOV 360 × 360 mm, matrix 320 × 320 mm, no interval scanning. In 1.5 T MRI, a total of eight images were obtained, with a scanning time of 63 s for each image post-contrast. Scanning parameters were as follows: TR 6.1 ms, TE 3.0 ms, FA 1.5°, FOV 330 × 330 mm.

2.4. Radiomics Analysis

2.4.1. Workflow

Radiomics analysis was performed using the uAI Research Portal (Shanghai United Imaging Intelligence Co., Ltd., China) embedded into the widely used package PyRadiomics (https://pyradiomics.readthedocs.io/en/latest/index.html) [11]. The radiomics workflow comprised tumor segmentation, feature extraction, feature selection, and model construction and evaluation (Figure 2).

To obtain as much effective information as possible from the limited data and to avoid possible sampling bias of grouping, this study adopted a five-fold cross-validation approach for modeling [26]. Specifically, the whole dataset was randomly, but equally, divided into five groups by unduplicated sampling, with the same ratio of LVI-positive patients in each group; training and validation were conducted on four groups and the remaining group, respectively, which was repeated until each group was used as validation data exactly once. Consequently, five models were generated, based on which an average but robust estimation could be obtained [26].

VOI, volumetric interest (volume of interest); LASSO, Least absolute shrinkage and selection operator; ROC, receiver operating characteristic curve; VOI tumor, the three-dimensional volume of the whole tumor; $VOI_{1\,mm}$, $VOI_{2\,mm}$, ..., and $VOI_{10\,mm}$, performing an isometric 3D expansion of the intratumoral region (VOI_{tumor}) from 1 mm to 10 mm resulted in the generation of regions including both the tumor and peritumor, which were labeled as $VOI_{1\,mm}$, $VOI_{2\,mm}$, ..., $VOI_{10\,mm}$ mm, respectively.

2.4.2. AI Tumor Segmentation

Zhang et al. [27] developed a spatial-temporal deep learning framework that integrates multi-phase dynamic contrast kinetics and spatial contextual features from DCE-MRI, enabling the model to simultaneously capture tumor enhancement patterns

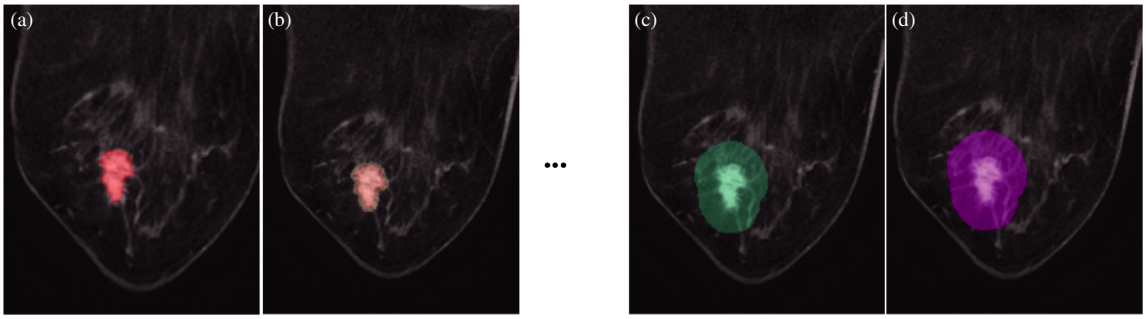

FIGURE 3. Automatic image segmentation example diagram. (a) VOI_{tumor}, the three-dimensional volume of the whole tumor; (b) $VOI_{1\,mm}$, an isometric 3D expansion of the intratumoral region 1 mm resulted in the generation of regions including both the tumor and the peritumor 1 mm; (c) $VOI_{9\,mm}$, an isometric 3D expansion of the intratumoral region 9 mm resulted in the generation of regions including both the tumor and the peritumor 9 mm; (d) $VOI_{10\,mm}$, an isometric 3D expansion of the intratumoral region 10 mm resulted in the generation of regions including both the tumor and the peritumor 10 mm.

and anatomical structures — thereby improving segmentation accuracy in complex backgrounds. This architecture achieved a Dice similarity coefficient (DSC) of 82.04% on a multi-center dataset while reducing segmentation time by 20-fold compared to manual methods, demonstrating physician-level accuracy alongside robust adaptability to MRI data with varying phase numbers and imaging intervals. In this study, we utilize an AI-assisted segmentation framework to extract tumor regions from DCE-MRI images across the second stages, thereby significantly reducing annotation time.

2.4.3. Image Processing

Analyses were conducted on the second phase of DCE-MRI [17]. Tumors were automatically segmented using an AI-assisted framework [12], followed by manual refinement on the original scans by a radiologist with three years of clinical experience in breast imaging. For patients with bilateral tumors, the larger lesion was selected for subsequent analysis.

To explore peritumoral information, a standard image morphological dilation operation was utilized to perform an isometric 3D expansion of the intratumoral region (volume of interest (VOI_{tumor})) from 1 mm to 10 mm. During this process, any area exceeding the bilateral breast region was eliminated. This resulted in the generation of regions, including both the tumor and peritumor, which were labeled as $VOI_{1\,mm}$, ..., $VOI_{9\,mm}$ and $VOI_{10\,mm}$, respectively (Figure 3).

2.4.4. Feature Extraction

To construct the optimal model, radiomics features were respectively derived from different VOIs (VOI_{tumor}, $VOI_{1\,mm}$, $VOI_{2\,mm}$, ..., $VOI_{10\,mm}$) in the DCE-MRI scans, which allowed for a comprehensive analysis of the radiomics characteristics within various regions of interest.

The images were imported into the uAI Research Portal, and a total of 104 radiomics features were extracted from within the annotated lesion region. These radiomics features included first-order statistics, shape, gray level cooccurrence matrix, gray level size zone matrix, gray level run length matrix, neighboring gray-tone difference matrix, and gray level dependence matrix features. Meanwhile, three imaging filters (original, log, wavelet) provided by the uAI Research Portal were utilized for feature extraction. Consequently, 1184 features were ultimately obtained for each of the VOI_{tumor} and $VOI_{1–10\,mm}$ subgroups.

2.4.5. Feature Selection

After maximum absolute value normalization, the least absolute shrinkage and selection operator regression were used to each feature. According to Harrell's guideline, the number of selected test features should be less than 10% of the sample size. Therefore, the number of features used for subsequent model construction was determined to be < 20 for each experiment.

2.4.6. Model Construction and Evaluation

Radiomics modeling was implemented based on VOI_{tumor}, $VOI_{1\,mm}$, $VOI_{2\,mm}$, ..., $VOI_{10\,mm}$, respectively. Machine-learning classifiers, including logistic regression and random forest, were utilized to build models after data preprocessing using the Box-Cox transformation. The radiomics model based on $VOI_{3\&4\,mm}$ refers to the model established on the combination of features extracted from $VOI_{3\,mm}$ and $VOI_{4\,mm}$, followed by feature extraction and model establishment. The 28 radiomics characteristics selected from $VOI_{3\,mm}$ and $VOI_{4\,mm}$ are in Figure 4.

Receiver operating characteristic curves were plotted, and AUC, accuracy, sensitivity, and specificity were calculated to quantify the predictive model performance. Afterward, calibration curves were plotted to estimate the coincidence between the prediction models and actual outcomes. Finally, decision curves were utilized to visualize the clinical net benefit of the prediction models.

3. STATISTICAL ANALYSIS

All statistical analyses were conducted using MedCalc (version 20.010; https://www.medcalc.org) and Python 3.7 software (https://www.python.org). Continuous variables and categorical variables were expressed as mean ± SD (standard devia-

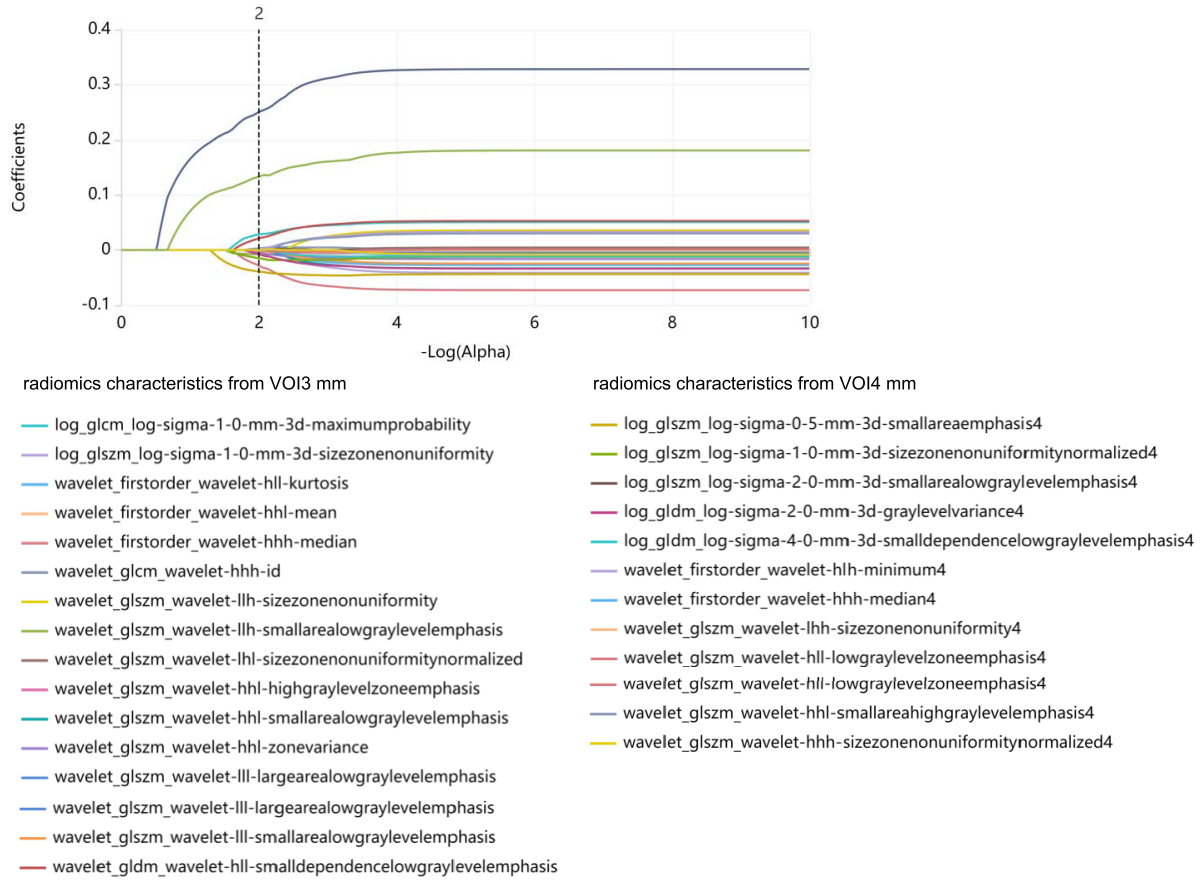

FIGURE 4. 28 radiomics features selected from $VOI_{3\,mm}$ and $VOI_{4\,mm}$, among which 16 features were from $VOI_{3\,mm}$ and 12 features were from $VOI_{4\,mm}$.

tion) and number (%), respectively. Clinical, pathological, and MRI findings were compared using the Wilcoxon rank sum test, Pearson Chi-square test, or Fisher's exact test. The consistency of the MRI findings was assessed by Kappa. The DeLong test was performed to compare AUCs. $P < 0.05$ was considered statistically significant.

4. RESULTS

4.1. Clinical Characteristics

A total of 193 patients with IBC met the inclusion criteria. The baseline characteristics of patients are summarized in Table 1. Among the patients, 143 were LVI-negative, and the other 50 were LVI-positive. There were no significant statistical differences between the groups in terms of age, histological grade, ER (estrogen receptors) status, PR (progesterone receptors) status, Ki67 level, and tumor sites, as well as tumor morphology, margin, boundary, and diameter on MRI. The chi-square test results showed that axillary lymph nodes (ALN) status, ALN status on MRI, and tumor enhancement pattern on MRI were significantly correlated to LVI ($P < 0.001$, $P = 0.005$, $P = 0.031$, respectively). The Kappa test between two observers indicated good consistency (Table 1).

Multivariable logistic regression analysis revealed that ALN enlargement is more common in LVI-positive patients than in LVI-negative patients (odds ratio [OR] $= 6.035$; 95% confidence interval [CI]: 1.801–20.221; $P = 0.004$) (Table 2). LVI-positive patients had a higher probability of annular enhancement pattern on MRI (OR $= 4.550$; 95% CI: 1.330–15.565; $P = 0.016$) than LVI-negative patients. Therefore, ALN status on MRI and tumor enhancement pattern on MRI were independent predictors of LVI. Based on this, a clinical model (training cohort, AUC: 0.655, 95% CI: 0.562–0.750; validation cohort, AUC: 0.644, 95% CI: 0.454–0.835) was established.

4.2. Performance of Intra- and Peritumoral Radiomics

After 5-fold cross-validation, the mean performance of the intra- and peritumoral 1–10 mm models for predicting LVI in the training and validation cohorts are shown in Tables 3 and 4. Among these models, the AUC value of the $VOI_{3\,mm}$ radiomics model was the highest but without statistical significance compared to that of the VOI_{tumor} radiomics model (AUCs: 0.891 vs. 0.853; $P = 0.330$) (Figures 5(a) and (b)). The AUC value of the $VOI_{4\,mm}$ radiomics model was 0.890, second only to the $VOI_{3\,mm}$ radiomics model (Figures 5(a) and (b)). Therefore, a combined radiomics model (referred to as $VOI_{3\&4\,mm}$) was constructed based on the selected 16 radiomics signatures from $VOI_{3\,mm}$ and 12 radiomics signatures from $VOI_{4\,mm}$. The model achieved an AUC of 0.951 (95% CI: 0.885–1.000), with sensitivity, specificity, and accuracy of 88.0%, 96.5%, and 84.3%,

TABLE 1. Clinical, histopathological and DCE-MRI characteristics of 193 lesions.

Characteristic	LVI negative ($n = 143$)	LVI positive ($n = 50$)	P value	Kappa
Age (y, mean ± SD)	51.63 ± 9.84	49.38 ± 9.94	0.900	\
Histological grade n (%)			0.197	\
I&II	92 (64.3)	27 (54.0)		
III	51 (35.7)	23 (46.0)		
ALN positive n (%)	55 (38.5)	39 (78.0)	$< 0.001*$	\
ER positive n (%)	108 (75.5)	36 (72.0)	0.623	\
PR positive n (%)	95 (66.4)	35 (70.0)	0.644	\
Ki 67 $\geq$ 14% n (%)	109 (76.2)	44 (88.0)	0.078	\
Right breast position n (%)	69 (48.3)	26 (52.0)	0.770	\
ALN status on MRI n (%)			0.005*	0.848
Normal	77 (53.9)	17 (34.0)		
Display	60 (42.0)	25 (50.0)		
Enlargement	6 (4.2)	8 (16.0)		
Tumor morphology on MRI n (%)			0.748	0.774
Cycle	17 (11.9)	4 (8.0)		
Oval	35 (24.5)	13 (26.0)		
Irregular	91 (63.6)	33 (66.0)		
Tumor margin on MRI n (%)			0.584	0.747
Smooth	24 (16.8)	11 (22.0)		
Lobular	65 (45.5)	19 (38.0)		
Spicule	54 (37.8)	20 (40.0)		
Tumor boundary on MRI n (%)			0.725	0.765
Sharp	56 (39.2)	21 (42.0)		
Fuzzy	87 (60.8)	29 (58.0)		
Tumor enhancement pattern on MRI n (%)			0.031*	0.875
Homogeneous	37 (25.9)	6 (12.0)		
Heterogeneous	93 (65.0)	34 (68.0)		
Annular	13 (9.1)	10 (20.0)		
Tumor diameter on MRI n (%)			0.491	0.886
< 2 cm	88 (61.5)	26 (52.0)		
$2 \sim 5$ cm	51 (35.7)	22 (44.0)		
> 5 cm	4 (2.8)	2 (4.0)		

Note — Data are number of lesions, and data in parentheses are percentages.
The differences were assessed by Mann-Whitney U-test, chi-square test, or chi-square test for trend. LVI, lymphovascular invasion; SD, standard deviation; ER, estrogen receptor; PR, progesterone receptor; ALN, axillary lymph node. *$P < 0.05$.

respectively (Figures 5(a) and (b)). The AUC value of the $VOI_{3\&4\,mm}$ radiomics model was significantly higher than that of the VOI_{tumor} radiomics model (AUCs: 0.951 vs. 0.853; $P = 0.003$), as well as the clinical model (AUCs: 0.951 vs. 0.644; $P < 0.001$) (Figures 5(a) and (b)). However, the AUC value of the comprehensive model combining clinical variables and $VOI_{3\&4\,mm}$ radiomics features was only 0.568. The decision curve (Figures 5(c) and (d)) shows that the $VOI_{3\&4\,mm}$ model added more clinical net benefit than the $VOI_{3\,mm}$ model. The calibration curve (Figures 5(e) and (f)) showed that $VOI_{3\&4\,mm}$ model is the best because it predicts the incidence closest to the measured incidence.

5. DISCUSSION

In this retrospective study, we developed a predictive model for LVI, based on the analysis of clinical characteristics, MRI findings, and DCE-MRI-based intra- and peritumoral radiomics features in patients with LVI-positive and LVI-negative IBC. Our results showed that the ALN status on MRI and the tumor enhancement pattern on MRI were independent predictors of LVI. The $VOI_{3\&4\,mm}$ radiomics model outperformed the VOI_{tumor} radiomics model, demonstrating that the radiomics features of intra- and peritumor can better predict the state of LVI than that of intratumor alone.

TABLE 2. Multivariable logistic regression analysis.

Characteristic	Odds ratio	95% CI	P value
ALN status on MRI			
Normal	Reference	...	...
Display	1.743	0.853 to 3.564	0.128
Enlargement	6.035	1.801 to 20.221	0.004*
Tumor enhancement pattern on MRI			
Homogeneous	Reference	...	...
Heterogeneous	2.217	0.836 to 5.877	0.11
Annular	4.55	1.330 to 15.565	0.016*

Note: 95% CI, 95% confidence interval. CI, confidence interval; ALN, axillary lymph node. *$P < 0.05$.

Our research suggests that the $VOI_{3\,mm}$ and $VOI_{4\,mm}$ radiomics models exhibited superior predictive capabilities. This could be attributed to the fact that a peritumor region of 3 mm or 4 mm radius encompasses significant information pertaining to surrounding blood vessels and lymphatic vessels while minimizing interference from irrelevant data [28]. As suggested by Ding et al. [28], optimizing the size of the area around the tumor can enhance the prediction accuracy of the radiomic model. Many studies [14, 29–32] have defined the area around the tumor as 4 mm, which is also in line with our research findings. The potential reasons for the relatively low performance of the other models are as follows: the prediction performance of the $VOI_{1\,mm}$ or $VOI_{2\,mm}$ radiomics models was lower than that of the $VOI_{3\,mm}$ radiomics model as they did not comprehensively include all important information. When the peritumoral expansion exceeds 4 mm, it not only includes all important information, such as surrounding blood vessels and lymphatic vessels, but also invalid information generated by normal breast tissue, which reduces the prediction efficiency of the models. The inferior performance of the combined model (clinical + radiomics, AUC $= 0.568$) compared to single-modality models highlights multifactorial mechanisms — including redundancy between clinical and radiomic features, suboptimal fusion strategies/methodological constraints, and heterogeneity in clinical data quality/completeness — as both explanatory factors and inherent limitations, urging future exploration of advanced multimodal integration techniques and rigorous data curation to mitigate such performance declines.

The presence of LVI serves as a valuable prognostic indicator for the likelihood of lymph node metastasis in breast cancer patients. A positive LVI result indicates an elevated risk of ALN metastasis and distant metastasis, both of which contribute to a poorer prognosis [3].

MRI has become one of the leading imaging methods for early screening, evaluation of malignancy, curative effects, and prognosis of breast cancer, especially DCE-MRI, which is considered to reflect lymphangiogenesis and microvessel density in breast cancer [33]. Previous studies [34, 35] have shown that some MRI findings are significantly correlated with LVI status. Cheon et al. [34] found that preoperative breast MRI findings, such as peritumoral and prothoracic edema, adjacent vascular signs, and regional enhancement on T2-weighted images, were associated with the presence of LVI. This is inconsistent with the results of Mori et al. [35], who found no significant relationship between LVI and T2WI, but found that the peritumor-to-tumor ADC ratio helped predict preoperative LVI status with good results (AUC: 0.81). In the current study, we only observed that the ALN status on MRI and the tumor enhancement pattern on MRI were independent predictors of LVI, while other features, such as peritumoral edema and adjacent vascular signs, were not significantly correlated with LVI. The AUC value of the clinical model based on ALN status and tumor enhancement pattern on MRI was 0.644. The significant variation in above several studies may result from the evaluations of different radiologists being, to some extent, subjective and may also be caused by the small sample size.

Therefore, more objective and reliable techniques, such as radiomics, are necessary for the preoperative prediction of LVI status in patients with breast cancer. Previous studies [10–13] have solely focused on the intratumoral area and have utilized one or more sequences from multi-parametric MRI imaging to establish radiomics models within tumors. For instance, Nijiati et al. [12] and Kayadibi et al. [13] have developed radiomics models based on ADC, achieving an AUC of 0.77 and 0.732, respectively. In addition, Liu et al. [10] have developed a radiomic model that is based on DCE-MRI, while Zhang et al. [11] have fused T2-weighted imaging (T2WI) and ADC images in their study. Previous MRI-based radiomics approaches on breast cancer suggested that the peritumoral area with 4 mm radial delineation distance outside breast cancer holds excellent information regarding the diagnosis of malignant lesions [36], prediction of lymph node metastasis status [28, 32], intraductal component [30], and assessment of molecular subtypes [31]. Li et al. [37] and Huang et al. [38]'s study of delineating the tumor and its peripheral area within 3 mm, including the microenvironment around the tumor, can provide rich information on tumor heterogeneity. Jiang et al. [17] developed a radiomics model based on intra- and peritumoral areas to evaluate LVI status, and they only tested 4 mm expansion, while in this study, the 1–10 mm gradient experiment proved that 3–4 mm was the optimal, and 3D isotropic expansion was adopted, which might

TABLE 3. The training cohorts' performances of the intratumoral and peritumoral 1 mm–10 mm models for predicting LVI.

Interest (VOI)	AUC (95% CI)	Sensitivity	Specificity	Accuracy
VOI_{tumor}	0.982(0.971–0.999)	0.955	0.872	0.894
$VOI_{1\ mm}$	0.993(0.994–1.000)	1.000	0.911	0.934
$VOI_{2\ mm}$	0.939(0.902–0.975)	0.88	0.85	0.858
$VOI_{3\ mm}$	0.969(0.947–0.993)	0.905	0.904	0.904
$VOI_{4\ mm}$	0.984(0.975–1.000)	0.955	0.871	0.892
$VOI_{5\ mm}$	0.957(0.931–0.986)	0.93	0.86	0.878
$VOI_{6\ mm}$	0.910(0.864–0.961)	0.785	0.832	0.82
$VOI_{7\ mm}$	0.901(0.848–0.956)	0.88	0.83	0.843
$VOI_{8\ mm}$	0.991(0.989–1.000)	0.925	0.974	0.961
$VOI_{9\ mm}$	0.985(0.976–1.000)	0.805	0.986	0.939
$VOI_{10\ mm}$	0.948(0.916–0.980)	0.85	0.941	0.917
$VOI_{3\&4\ mm}$	0.994(0.997–1.000)	0.96	0.984	0.978

Note: VOI, volumetric interest (volume of interest); VOI_{tumor}, the three-dimensional volume of the whole tumor; $VOI_{1\ mm}$, $VOI_{2\ mm}$, ..., and $VOI_{10\ mm}$, performing an isometric 3D expansion of the intratumoral region (VOI_{tumor}) from 1 mm to 10 mm resulted in the generation of regions including both the tumor and the peritumor, which were labeled as $VOI_{1\ mm}$, $VOI_{2\ mm}$, ..., and $VOI_{10\ mm}$ mm, respectively $VOI_{3\&4\ mm}$ refers to the model established on the combination of features extracted from $VOI_{3\ mm}$ and $VOI_{4\ mm}$.

TABLE 4. The validation cohorts' performances of the intratumoral and peritumoral 1 mm–10 mm models for predicting LVI.

Interest (VOI)	AUC (95% CI)	Sensitivity	Specificity	Accuracy
VOI_{tumor}	0.853(0.736–0.966)	0.8	0.796	0.798
$VOI_{1\ mm}$	0.816(0.676–0.957)	0.716	0.742	0.735
$VOI_{2\ mm}$	0.833(0.694–0.963)	0.76	0.811	0.798
$VOI_{3\ mm}$	0.891(0.786–0.994)	0.82	0.868	0.855
$VOI_{4\ mm}$	0.890(0.770–0.999)	0.84	0.833	0.834
$VOI_{5\ mm}$	0.826(0.686–0.967)	0.72	0.784	0.767
$VOI_{6\ mm}$	0.803(0.625–0.973)	0.74	0.804	0.787
$VOI_{7\ mm}$	0.855(0.714–0.993)	0.8	0.818	0.814
$VOI_{8\ mm}$	0.828(0.690–0.964)	0.58	0.882	0.803
$VOI_{9\ mm}$	0.836(0.690–0.979)	0.48	0.902	0.793
$VOI_{10\ mm}$	0.802(0.625–0.959)	0.62	0.888	0.818
$VOI_{3\&4\ mm}$	0.951(0.885–1.000)	0.88	0.965	0.843

Note: VOI, volumetric interest (volume of interest); VOI_{tumor}, the three-dimensional volume of the whole tumor; $VOI_{1\ mm}$, $VOI_{2\ mm}$, ..., and $VOI_{10\ mm}$ mm, performing an isometric 3D expansion of the intratumoral region (VOI_{tumor}) from 1 mm to 10 mm resulted in the generation of regions including both the tumor and the peritumor, which were labeled as $VOI_{1\ mm}$, $VOI_{2\ mm}$, ..., and $VOI_{10\ mm}$, respectively $VOI_{3\&4\ mm}$ refers to the model established on the combination of features extracted from $VOI_{3\ mm}$ and $VOI_{4\ mm}$.

be more in line with the stereospatial characteristics of tumor invasion.

Our research has some advantages. Firstly, the LVI status is predicted based on the radiomics of multiple intratumoral and peritumoral regions (1 mm, 2 mm, ..., and 10 mm, respectively). Secondly, the regions of interest were delineated semi-automatically, saving time and labor for clinical application.

Previous research reported that YOLOv8 model improves the accuracy of automatic detection of brain tumors in MRI [39]. Low-profile tapered slot ultra-wideband (UWB) Vivaldi antenna is applicable to breast cancer diagnosis [40].

There are some limitations. First, there is a potential impact of category imbalance between the training set and validation set in this study (50 LVI-positive patients among the total 193 patients), so we ensured the consistency of the category ratio of the training/validation set in 5-times cross-validation through stratified sampling). Although the current AUC value is very high, it is still necessary to suggest future large-sample validation. Second, the underperformance of the combined model

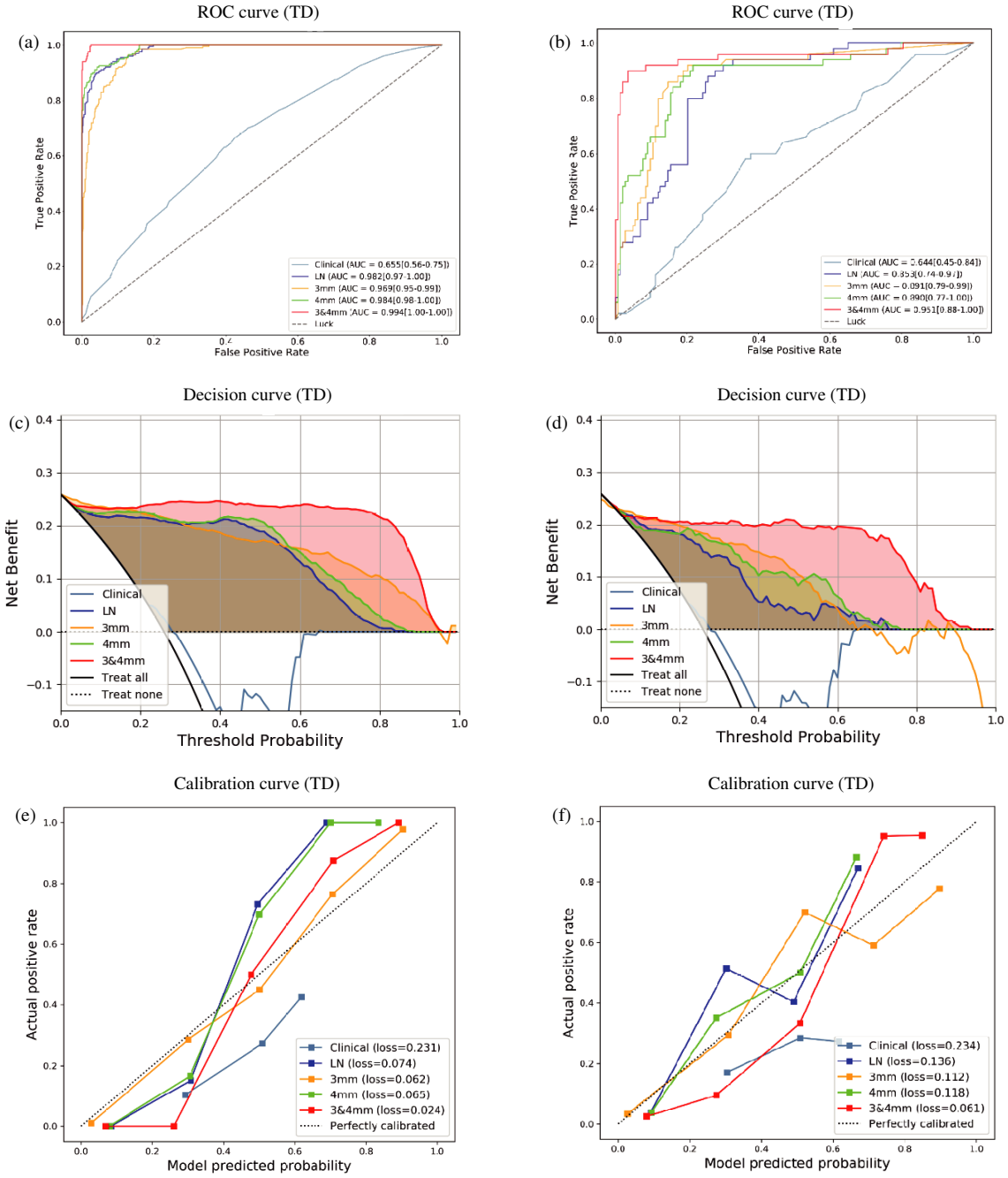

FIGURE 5. The performance of the clinical model and VOI_{tumor}, $VOI_{3\,mm}$, $VOI_{4\,mm}$, and $VOI_{3\&4\,mm}$ radiomics models were assessed using ROC curves, decision curves, and calibration curves of LVI. (a), (b) The ROC, (c), (d) calibration, and (e), (f) decision curves of different models for predicting LVI in the training dataset and validation dataset. ROC, receiver operating characteristic; LVI, lymphatic vascular invasion; TD, training dataset; VD, validation dataset.

(clinical + radiomics, AUC = 0.568) stems from feature redundancy, imperfect fusion methods, and data heterogeneity, emphasizing the need for advanced multimodal frameworks and standardized clinical data protocols in future studies. Third, this study was a retrospective single-center study, and multicenter studies and external datasets are still needed to verify generalizability. Furthermore, the use of DCE-MRI may only miss complementary information from ADC or T2WI, and the integration of multiple sequence features is needed to improve robustness in the future.

6. CONCLUSION

Intra- and peritumoral radiomics based on DCE-MRI can effectively predict the LVI status of IBC, compared to intratumoral radiomics alone. Moreover, the predictive performance of the radiomics model might be further improved by optimizing the size of the peritumoral area, with an optimal size of 3–4 mm.

REFERENCES

[1] Bray, F., M. Laversanne, H. Sung, J. Ferlay, R. L. Siegel, I. Soerjomataram, and A. Jemal, "Global cancer statistics 2022:

GLOBOCAN estimates of incidence and mortality worldwide for 36 cancers in 185 countries," *CA: A Cancer Journal for Clinicians*, Vol. 74, No. 3, 229–263, 2024.

[2] Hwang, K.-T., Y. A. Kim, J. Kim, A. J. Chu, J. H. Chang, S. W. Oh, K. R. Hwang, and Y. J. Chai, "The influences of peritumoral lymphatic invasion and vascular invasion on the survival and recurrence according to the molecular subtypes of breast cancer," *Breast Cancer Research and Treatment*, Vol. 163, 71–82, 2017.

[3] Ejlertsen, B., M.-B. Jensen, F. Rank, B. B. Rasmussen, P. Christiansen, N. Kroman, M. E. Kvistgaard, M. Overgaard, D. B. Toftdahl, H. T. Mouridsen, *et al.*, "Population-based study of peritumoral lymphovascular invasion and outcome among patients with operable breast cancer," *JNCI: Journal of the National Cancer Institute*, Vol. 101, No. 10, 729–735, 2009.

[4] Yi, M., E. A. Mittendorf, J. N. Cormier, T. A. Buchholz, K. Bilimoria, A. A. Sahin, G. N. Hortobagyi, A. M. Gonzalez-Angulo, S. Luo, A. U. Buzdar, *et al.*, "Novel staging system for predicting disease-specific survival in patients with breast cancer treated with surgery as the first intervention: Time to modify the current American joint committee on cancer staging system," *Journal of Clinical Oncology*, Vol. 29, No. 35, 4654–4661, 2011.

[5] Rakha, E. A., S. Martin, A. H. S. Lee, D. Morgan, P. D. P. Pharoah, Z. Hodi, D. MacMillan, and I. O. Ellis, "The prognostic significance of lymphovascular invasion in invasive breast carcinoma," *Cancer*, Vol. 118, No. 15, 3670–3680, 2012.

[6] Schoppmann, S. F., G. Bayer, K. Aumayr, S. Taucher, S. Geleff, M. Rudas, E. Kubista, H. Hausmaninger, H. Samonigg, M. Gnant, *et al.*, "Prognostic value of lymphangiogenesis and lymphovascular invasion in invasive breast cancer," *Annals of Surgery*, Vol. 240, No. 2, 306–312, 2004.

[7] Viale, G., A. Giobbie-Hurder, B. A. Gusterson, E. Maiorano, M. G. Mastropasqua, A. Sonzogni, E. Mallon, M. Colleoni, M. Castiglione-Gertsch, M. M. Regan, *et al.*, "Adverse prognostic value of peritumoral vascular invasion: Is it abrogated by adequate endocrine adjuvant therapy? Results from two International Breast Cancer Study Group randomized trials of chemoendocrine adjuvant therapy for early breast cancer," *Annals of Oncology*, Vol. 21, No. 2, 245–254, 2010.

[8] Colleoni, M., N. Rotmensz, P. Maisonneuve, A. Sonzogni, G. Pruneri, C. Casadio, A. Luini, P. Veronesi, M. Intra, V. Galimberti, *et al.*, "Prognostic role of the extent of peritumoral vascular invasion in operable breast cancer," *Annals of Oncology*, Vol. 18, No. 10, 1632–1640, 2007.

[9] Yu, Y., Z. He, J. Ouyang, Y. Tan, Y. Chen, Y. Gu, L. Mao, W. Ren, J. Wang, L. Lin, *et al.*, "Magnetic resonance imaging radiomics predicts preoperative axillary lymph node metastasis to support surgical decisions and is associated with tumor microenvironment in invasive breast cancer: A machine learning, multicenter study," *EBioMedicine*, Vol. 69, 103460, 2021.

[10] Liu, Z., B. Feng, C. Li, Y. Chen, Q. Chen, X. Li, J. Guan, X. Chen, E. Cui, R. Li, *et al.*, "Preoperative prediction of lymphovascular invasion in invasive breast cancer with dynamic contrast-enhanced-MRI-based radiomics," *Journal of Magnetic Resonance Imaging*, Vol. 50, No. 3, 847–857, 2019.

[11] Zhang, J., G. Wang, J. Ren, Z. Yang, D. Li, Y. Cui, and X. Yang, "Multiparametric MRI-based radiomics nomogram for preoperative prediction of lymphovascular invasion and clinical outcomes in patients with breast invasive ductal carcinoma," *European Radiology*, Vol. 32, No. 6, 4079–4089, 2022.

[12] Nijiati, M., D. Aihaiti, A. Huojia, A. Abulizi, S. Mutailifu, N. Rouzi, G. Dai, and P. Maimaiti, "MRI-based radiomics for preoperative prediction of lymphovascular invasion in patients with invasive breast cancer," *Frontiers in Oncology*, Vol. 12, 876624, 2022.

[13] Kayadibi, Y., B. Kocak, N. Ucar, Y. N. Akan, E. Yildirim, and S. Bektas, "MRI radiomics of breast cancer: Machine learning-based prediction of lymphovascular invasion status," *Academic Radiology*, Vol. 29, S126–S134, 2022.

[14] Li, C., L. Song, and J. Yin, "Intratumoral and peritumoral radiomics based on functional parametric maps from breast DCE-MRI for prediction of HER-2 and Ki-67 status," *Journal of Magnetic Resonance Imaging*, Vol. 54, No. 3, 703–714, 2021.

[15] Zhang, S., X. Wang, Z. Yang, Y. Zhu, N. Zhao, Y. Li, J. He, H. Sun, and Z. Xie, "Intra- and peritumoral radiomics model based on early DCE-MRI for preoperative prediction of molecular subtypes in invasive ductal breast carcinoma: A multitask machine learning study," *Frontiers in Oncology*, Vol. 12, 905551, 2022.

[16] Zhan, C., Y. Hu, X. Wang, H. Liu, L. Xia, and T. Ai, "Prediction of axillary lymph node metastasis in breast cancer using intra-peritumoral textural transition analysis based on dynamic contrast-enhanced magnetic resonance imaging," *Academic Radiology*, Vol. 29, S107–S115, 2022.

[17] Jiang, W., R. Meng, Y. Cheng, H. Wang, T. Han, N. Qu, T. Yu, Y. Hou, and S. Xu, "Intra- and peritumoral based radiomics for assessment of Lymphovascular invasion in invasive breast cancer," *Journal of Magnetic Resonance Imaging*, Vol. 59, No. 2, 613–625, 2024.

[18] Lee, C.-Y., T.-F. Chang, N.-Y. Chang, and Y.-C. Chang, "An automated skin segmentation of breasts in dynamic contrast-enhanced magnetic resonance imaging," *Scientific Reports*, Vol. 8, No. 1, 6159, 2018.

[19] Khaled, R., J. Vidal, J. C. Vilanova, and R. Martí, "A U-Net Ensemble for breast lesion segmentation in DCE MRI," *Computers in Biology and Medicine*, Vol. 140, 105093, 2022.

[20] Si, T., D. K. Patra, S. Mondal, and P. Mukherjee, "Breast DCE-MRI segmentation for lesion detection using chimp optimization algorithm," *Expert Systems with Applications*, Vol. 204, 117481, 2022.

[21] Wang, S., K. Sun, L. Wang, L. Qu, F. Yan, Q. Wang, and D. Shen, "Breast tumor segmentation in DCE-MRI with tumor sensitive synthesis," *IEEE Transactions on Neural Networks and Learning Systems*, Vol. 34, No. 8, 4990–5001, 2023.

[22] Si, T. and A. Mukhopadhyay, "Breast DCE-MRI segmentation for lesion detection using clustering with fireworks algorithm," in *Applications of Artificial Intelligence in Engineering*, 17–35, 2021.

[23] Du, Y., M. Cai, H. Zha, B. Chen, J. Gu, M. Zhang, W. Liu, X. Liu, X. Liu, M. Zong, and C. Li, "Ultrasound radiomics-based nomogram to predict lymphovascular invasion in invasive breast cancer: A multicenter, retrospective study," *European Radiology*, Vol. 34, No. 1, 136–148, 2024.

[24] Houvenaeghel, G., M. Cohen, J. M. Classe, F. Reyal, C. Mazouni, N. Chopin, A. Martinez, E. Daraï, C. Coutant, P. E. Colombo, *et al.*, "Lymphovascular invasion has a significant prognostic impact in patients with early breast cancer, results from a large, national, multicenter, retrospective cohort study," *ESMO Open*, Vol. 6, No. 6, 100316, 2021.

[25] Elston, C. W. and I. O. Ellis, "Pathological prognostic factors in breast cancer. I. The value of histological grade in breast cancer: Experience from a large study with long-term follow-up," *Histopathology*, Vol. 19, No. 5, 403–410, 1991.

[26] Chong, H., Y. Gong, X. Pan, A. Liu, L. Chen, C. Yang, and M. Zeng, "Peritumoral dilation radiomics of gadoxetate disodium-enhanced MRI excellently predicts early recurrence of hepatocellular carcinoma without macrovascular invasion af-

ter hepatectomy," *Journal of Hepatocellular Carcinoma*, Vol. 8, 545–563, 2021.

[27] Zhang, J., Z. Cui, Z. Shi, Y. Jiang, Z. Zhang, X. Dai, Z. Yang, Y. Gu, L. Zhou, C. Han, *et al.*, "A robust and efficient AI assistant for breast tumor segmentation from DCE-MRI via a spatial-temporal framework," *Patterns*, Vol. 4, No. 9, 100826, 2023.

[28] Ding, J., S. Chen, M. S. Sosa, R. Cattell, L. Lei, J. Sun, P. Prasanna, C. Liu, and C. Huang, "Optimizing the peritumoral region size in radiomics analysis for sentinel lymph node status prediction in breast cancer," *Academic Radiology*, Vol. 29, S223–S228, 2022.

[29] Jiang, T., J. Song, X. Wang, S. Niu, N. Zhao, Y. Dong, X. Wang, Y. Luo, and X. Jiang, "Intratumoral and peritumoral analysis of mammography, tomosynthesis, and multiparametric MRI for predicting Ki-67 level in breast cancer: A radiomics-based study," *Molecular Imaging and Biology*, Vol. 24, 550–559, 2022.

[30] Xu, H., J. Liu, Z. Chen, C. Wang, Y. Liu, M. Wang, P. Zhou, H. Luo, and J. Ren, "Intratumoral and peritumoral radiomics based on dynamic contrast-enhanced MRI for preoperative prediction of intraductal component in invasive breast cancer," *European Radiology*, Vol. 32, No. 7, 4845–4856, 2022.

[31] Niu, S., W. Jiang, N. Zhao, T. Jiang, Y. Dong, Y. Luo, T. Yu, and X. Jiang, "Intra- and peritumoral radiomics on assessment of breast cancer molecular subtypes based on mammography and MRI," *Journal of Cancer Research and Clinical Oncology*, Vol. 148, 97–106, 2022.

[32] Liu, C., J. Ding, K. Spuhler, Y. Gao, M. S. Sosa, M. Moriarty, S. Hussain, X. He, C. Liang, and C. Huang, "Preoperative prediction of sentinel lymph node metastasis in breast cancer by radiomic signatures from dynamic contrast-enhanced MRI," *Journal of Magnetic Resonance Imaging*, Vol. 49, No. 1, 131–140, 2019.

[33] Poellinger, A., S. El-Ghannam, S. Diekmann, T. Fischer, G. Kristiansen, F. Fritzsche, E. Fallenberg, L. Morawietz, and F. Diekmann, "Correlation between enhancement characteristics of MR mammography and capillary density of breast lesions," *European Journal of Radiology*, Vol. 83, No. 12, 2129–2136, 2014.

[34] Cheon, H., H. J. Kim, S. M. Lee, S. H. Cho, K. M. Shin, G. C. Kim, J. Y. Park, and W. H. Kim, "Preoperative MRI features associated with lymphovascular invasion in node-negative invasive breast cancer: A propensity-matched analysis," *Journal of Magnetic Resonance Imaging*, Vol. 46, No. 4, 1037–1044, 2017.

[35] Mori, N., S. Mugikura, C. Takasawa, M. Miyashita, A. Shimauchi, H. Ota, T. Ishida, A. Kasajima, K. Takase, T. Kodama, and S. Takahashi, "Peritumoral apparent diffusion coefficients for prediction of lymphovascular invasion in clinically node-negative invasive breast cancer," *European Radiology*, Vol. 26, 331–339, 2016.

[36] Zhou, J., Y. Zhang, K.-T. Chang, K. E. Lee, O. Wang, J. Li, Y. Lin, Z. Pan, P. Chang, D. Chow, *et al.*, "Diagnosis of benign and malignant breast lesions on DCE-MRI by using radiomics and deep learning with consideration of peritumor tissue," *Journal of Magnetic Resonance Imaging*, Vol. 51, No. 3, 798–809, 2020.

[37] Li, J., Z. Qiu, C. Zhang, S. Chen, M. Wang, Q. Meng, H. Lu, L. Wei, H. Lv, W. Zhong, and X. Zhang, "ITHscore: Comprehensive quantification of intra-tumor heterogeneity in NSCLC by multi-scale radiomic features," *European Radiology*, Vol. 33, No. 2, 893–903, 2023.

[38] Huang, Y., X. Wang, Y. Cao, X. Lan, X. Hu, F. Mou, H. Chen, X. Gong, L. Li, S. Tang, *et al.*, "Nomogram for predicting neoadjuvant chemotherapy response in breast cancer using mri-based intratumoral heterogeneity quantification," *Radiology*, Vol. 315, No. 1, e241805, 2025.

[39] Lin, Z., W. Lin, and F. Jiang, "YOLOv8-DEC: enhancing brain tumor object detection accuracy in magnetic resonance imaging," *Progress In Electromagnetics Research M*, Vol. 129, 43–52, 2024.

[40] Sasikala, S., K. Karthika, S. Arunkumar, K. Anusha, S. Adithya, and A. J. A. Al-Gburi, "Design and analysis of a low-profile tapered slot uwb vivaldi antenna for breast cancer diagnosis," *Progress In Electromagnetics Research M*, Vol. 124, 43–51, 2024.